## Geophysical Journal International



doi: 10.1093/gji/ggz252

Geophys. J. Int. (2019) **218**, 1796–1806 Advance Access publication 2019 May 31 GJI Geomagnetism, rock magnetism and palaeomagnetism

# Solving the mystery of the 1960 Hawaiian lava flow: implications for estimating Earth's magnetic field

### J. Michael Grappone <sup>10</sup>, Andrew J. Biggin and Mimi J. Hill

Geomagnetism Laboratory, School of Environmental Sciences, University of Liverpool, Liverpool L69 7ZE, UK. E-mail: jmgrappone@gmail.com

Accepted 2019 May 30. Received 2019 May 15; in original form 2018 September 26

### SUMMARY

Studying historic lava flows provides a rare comparison between direct measurements of the Earth's magnetic field and the field information recorded in the rock record. Connecting direct and indirect measurements provides a way to bridge the gap between historic data in the last 50-100 yr to geologic data over kyr to Gyr. The field strength in Hawaii in 1960 was directly measured at the Honolulu observatory to be 36.47 μT, so our palaeointensity analysis of the 1960 flow is expected to give the same value. Two vertical sections of the 1960 flow (section 1 and section 2) were the focus of a previous microwave palaeointensity study. The microwave experiments were run using the non-standard, perpendicular modified Thellier-type protocol and produced either apparently good quality data that were biased to low values (section 1) or more scattered results averaging close to the expected value (section 2). The cause of the non-ideal behaviour observed in the data from the 1960 flow is a long-standing mystery that it is important to resolve to confirm the reliability of palaeointensity measurements in general, and the microwave demagnetization mechanism in particular. Here, we test the hypothesis that higher quality, unbiased (only random noise) measurements are possible using an improved Thellier-type protocol coupled to an updated microwave system. New palaeointensity experiments were performed primarily using the IZZI protocol (which allows alteration checks during the experiment) adapted for the microwave system. The specimens from section 1 produced more linear Arai plots and gave an estimate of  $36.8 \pm 3.4 \mu T$ , whereas those from section 2 gave an estimate of 39.1  $\pm$  4.6  $\mu$ T. Our new experiments demonstrate the microwave system's ability to produce accurate results and efficiently run any Thellier-style experiment. We investigate correcting perpendicular data for undetected alteration and find that using too strict selection criteria can be counterproductive to obtaining accurate and precise microwave palaeointensity results.

**Key words:** Palaeointensity; Palaeomagnetism; Remagnetization.

### 1 INTRODUCTION

Understanding the Earth's magnetic field is key to understanding the behaviour of the Earth's interior. Satellites give us extensive data on the geomagnetic field for the last 30–40 yr and ground-based observatories (such as the Honolulu observatory or the French Bureau Central de Magnétisme Terrestre) provide data for up to an additional 100 yr (Jackson *et al.* 2000). Palaeomagnetic techniques let us extend these data to Gyr timescales. Palaeomagnetic investigation of the rock record allows surface measurements that, given suitable rocks, can be used to provide insight into deep Earth processes at any point in geologic time.

Lavas contain magnetic field information stored in the magnetic grains of which the most common is (titano)magnetite. Palaeointensities (PIs) cannot be directly measured *in situ*, however. In order to

extract PI estimates, we must subject specimens to extensive experiments, whose accuracies are the subject of some debate (Donadini *et al.* 2007; Biggin 2010; Cromwell *et al.* 2018). Data from historic lava flows, like those in Hawaii, therefore allow us to test various PI methods on many rock types, since the answer is already known. In addition, the data allow geomagnetic models to connect the modern, continuous data records with the discrete data sets that volcanic eruptions provide.

One of the most important places for palaeomagnetism is the Hawaiian Island chain. The island of Hawaii has active volcanoes and is located in the middle of the central Pacific, which covers 30 per cent of the Earth's surface. In 1960, Kilauea's east rift zone erupted. The proximity of this site to the Honolulu Observatory (370 km away) provides a close approximation (36.47  $\mu$ T) of the magnetic field intensity at the eruption site (Tanaka & Kono 1991;

Böhnel *et al.* 2011). Coe & Gromme (1973) suggested that the local magnetic field at the volcano could deviate from the observatory data by up to  $\pm 2~\mu T$ . The International Geomagnetic Reference Field:  $12^{th}$  Edition (IGRF-12; Thebault *et al.* 2015) provides a second estimate of 36.2  $\mu T$ , with the caveat that small-scale magnetic anomalies can go undetected (Coe & Gromme 1973).

Previous study-level average PI estimates (e.g. Hill & Shaw 2000; Böhnel et al. 2011; Cromwell et al. 2015; Yamamoto et al. 2003) range from 33.9 μT using the microwave-perpendicular (MW-Perp) method in Hill & Shaw (2000) to 49.0 μT using the Thellier-Coe method in Yamamoto et al. (2003). Detailed analyses of previous palaeodirection studies, which show a recorded modern field direction, and PI studies on the 1960 lava flow are given in Böhnel et al. (2011) and Cromwell et al. (2015). Herrero-Bervera & Valet (2009) extracted a highly accurate (<2 per cent error) PI estimate of 36.9 μT, using a (relatively large) set of 36 specimens. Cromwell et al. (2015) similarly obtained an accurate estimate of 36.0 μT, using very strict selection criteria, which resulted in a success rate of 38 per cent (7/18). In the previous MW study, Hill & Shaw (2000) used the non-standard perpendicular protocol out of necessity because the early 8.2 GHz MW system had poor power absorption reproducibility precluding both double treatments and alteration checks. For section 1, their data gave linear Arai plots, with a mean  $\beta$  (relative standard error) of 0.027, whose estimates were around 13 per cent lower than expected, at  $31.6 \pm 3.6 \mu$ T. At section 2, the Arai plots showed considerable nonlinear, two-slope behaviour, but an (accurate) estimate of  $37.1 \pm 6.4 \mu T$  was extracted by fitting the entire Arai plot, regardless of linearity. This result is unexpected, as more linear (less noisy) data would be expected to be more accurate than less ideal (noisier) data.

These previous studies found significant variations in magnetic properties throughout the 1960 lava flow both vertically and laterally. Previously reported scanning electron microscopy shows elongated primary low-Ti titanomagnetite, which forms during cooling and thus retains a thermoremanent magnetization (TRM; Dunlop & Ozdemir 2001; Böhnel et al. 2011). Yamamoto et al. (2003) determined that alterations leading to a thermochemical remanent magnetization (TCRM) can explain why many thermal studies give high PI estimates. Generally, studies that used more specimens had estimates closer to the expected value, which suggests that either the flow has significant heterogeneities across it (a point noted in Hill & Shaw 2000) or the PI methods used are inherently noisy. We note both of these explanations can be remedied by more extensive sampling of a given lava flow, since sparse sampling of heterogeneous flows can exaggerate the contribution of non-random (biased) noise in the data. Exaggerated non-single domain contributions can cause systematic differences in estimates for single- and double-treatment protocols (Biggin 2010). The cause of the non-ideal behaviour in these rocks, however, has been a mystery for over 20 yr.

Hill & Shaw (2000) undertook extensive reflected-light microscopy and obtained hysteresis properties, isothermal remanent magnetization acquisitions and Curie curves for sister samples to those used herein. Hill & Shaw (2000) found in both sections predominantly titanomagnetite with a Curie temperature of approximately 520 °C. They further found predominately linear Curie curves, which imply rapid cooling of the lava, preventing uniform iron oxide grain distribution. Fig. 3 in Hill & Shaw (2000) shows moderately low (broadly between the single- and multidomain ranges) hysteresis parameters, with section 2 having a larger range than section 1. Rapidly cooled pseudo-single-domain grains typical of basalts have been shown to have negligible cooling rate effects (Yu 2011; Biggin et al. 2013; Ferk et al. 2014); however,

this has become the subject of some debate (Santos & Tauxe 2019). The previous MW data set from Hill & Shaw (2000) gave underestimates, which has the opposite sense to that expected if a cooling rate correction were needed. Cooling rate correction has, therefore, not been investigated in this study.

Advances in the MW technique now allow the use of the IZZI protocol (Yu et al. 2004), which allows pT<sub>(M)</sub>RM [partial (microwave-) thermoremanent magnetization] checks for alteration and contains a built-in check for multidomain behaviour, through the zigzagging of the Arai plots (Yu & Tauxe 2005). We need to understand if using the more modern IZZI protocol helps resolve the unexpected outcome from Hill & Shaw (2000) to solidify the utility of not only the MW system but also the IZZI protocol applied to the MW. Our goal herein is, therefore, to extract high-quality PI data that yield an estimate of 36.2–36.5  $\mu T$  using Liverpool's most sophisticated MW system (Hill et al. 2008). We also aim, more generally, to determine the source of the non-ideal behaviour to confirm the reliability of PI measurements in general, and the MW system as a demagnetization mechanism in particular.

### 2 METHODS

The samples used are the archived samples remaining from Hill & Shaw (2000). In the original study, standard 25 mm diameter cores were taken from two sites, which were 16 m apart. At section 1, the flow was 1 m in height. At section 2, the flow was 75 cm in height. For full details, readers are referred to Hill & Shaw (2000). Due to the scarcity of material available, MW with a diameter of 5 mm and a height of 1–2 mm (instead of the more standard 5 mm height) were drilled from 21 individual 25 mm diameter cores to maximize the number of specimens.

The main protocol used in this study was the IZZI protocol (Yu et al. 2004), adapted for use on the MW system, which we ran on 59 specimens. To compare our data to the previous study, we also used the MW-Perp method (Hill & Shaw 2007) on 46 specimens of which 21 also included pT<sub>M</sub>RM checks. All MW tests were run on the 14 GHz Tristan MW system at the University of Liverpool's Geomagnetism Laboratory (Hill et al. 2008). We used MW powers starting at 5 W for 5 s, up to the maximum of 40 W, for a maximum time of 20 s (normally 5–8 s maximum), generally until specimens have lost at least 90 per cent of their Natural Remanent Magnetization (NRM). We used an applied laboratory field of 36  $\mu$ T, approximately the expected strength. The field was always applied perpendicular to the specimen's NRM. This can exaggerate Arai plot zigzagging (Yu & Tauxe 2005) from specimens that contain non-SD magnetic grains, according to Shaar et al. (2011), but it allows a more direct comparison with Hill & Shaw (2000).

The IZZI protocol is a double-treatment protocol that combines in-field (I) steps and zero-field (Z) steps in an enclosed couplet. At each MW power integral, both a Z and an I step are performed before being taken to a higher power integral and the treatments reversed. We used the variant ZIIZ, followed by a pT<sub>M</sub>RM check step (P) with the same power integral as the last step in the previous couplet, which gives a complete pattern of 'ZIIZP'. The standard IZZI protocol includes pTRM checks (Yu *et al.* 2004), but it can, in theory, be run without them. Therefore, for consistency and clarity with the other protocols used, in this paper, we will refer to the MW version of IZZI with pT<sub>M</sub>RM checks as MW-IZZI+.

The perpendicular protocol (Kono & Ueno 1977) uses only a single treatment at each temperature step, with the field applied perpendicular to the specimen's NRM. Variation from a perpendicularly applied field is represented by  $\Delta\theta$  and is required to be small. For 21 specimens, we also included a Z step and a P step after every other I step. The Z step is necessary for the pT<sub>M</sub>RM check to work. With the addition of the Z and P steps, this protocol can be written as 'IIZP'. We will refer to this protocol as MW-Perp++ to reflect the additional two steps. We note that Biggin (2010) predicted that the addition of Z and P steps to a perpendicular experiment would add considerable extra data point scatter on Arai plots if the remanence carriers do not behave as ideal single-domain grains.

In this paper, we use a primary, moderately strict, set of selection criteria, modelled after the MC-CRIT.C1 selection criteria (without tail checks) from Paterson *et al.* (2015). To test the influence of selection criteria on the PI estimates, we also tested two additional sets of selection criteria on the MW-IZZI+ data analysis: a loose set modelled after Bono *et al.* (2019) and a strict set modelled after Cromwell *et al.* (2015). These criteria can be found in Table 1. Paterson *et al.* (2015) details the statistics and showed that the moderately strict selection criteria have a median accuracy of 95.3 per cent in their experiments (with tail checks). In all cases, in order to try to minimize the impact of estimates made from lower power integral steps, we opted for the longest best-fit line that still passed the selection criteria.

First Order Reversal Curves (FORCs) were run on two specimens to assess their magnetic domain states. The data were gathered on a Princeton Instruments Vibrating Sample Magnetometer (VSM) at the Institute of Rock Magnetism (IRM) at the University of Minnesota. These data are available in Supporting Information Section A.

We were also interested in correlating changes in hysteresis parameters with pT<sub>M</sub>RM check failures. To do this, we ran hysteresis loops on a Magnetic Measurements Variable Field Transition Balance to compare changes in hysteresis parameters with the failure of pT<sub>M</sub>RM checks. We used sister specimens of those used in the PI experiments. We ran an initial hysteresis loop, then simulated an MW-IZZI+ experiment, completing the ZIIZP pattern at the same powers used on sister PI experiment specimens. Another hysteresis loop was measured, and then the specimen underwent another ZIIZP at the next power integral steps.

### 3 RESULTS

### 3.1 Palaeointensity estimates

We ran 70 specimens from 13 samples from section 1 and 35 specimens from 8 samples from section 2. Using our preferred selection criteria, the moderately strict set, 68 new PI estimates were accepted, for an overall success rate of 65 per cent. All new PI estimates and raw data will be available on the MagIC database. Arai plot fit data can be found in Supporting Information B. Some specimens showed an overprint removed at low power integrals, but the additional component generally disappeared by power integral applications of approximately 40–60 Ws. No systematic variation was observed over the available sampling of the section. We therefore report an arithmetic mean and one standard deviation of the successful specimens' PI estimates, in Table 2. Most specimens lost the majority of their magnetization by 1600 Ws. It was necessary, however, to treat some (usually in one or two large steps) to  $\sim$ 2400 Ws.

### 3.1.1 Section 1

Of the 41 specimens that underwent an MW-IZZI+ treatment, 70 per cent passed the loose selection criteria and averaged  $37.3 \pm 3.3 \,\mu\text{T}$ , 54 per cent passed the moderately strict selection criteria and averaged  $36.8 \pm 3.4 \,\mu\text{T}$  and 0 per cent passed the strict selection criteria. The loose and moderately strict estimates are not statistically distinct from the IGRF field estimate of 36.2  $\mu$ T, with p = 0.20 and p = 0.68, respectively. The most common reason for failure for the MW-IZZI+ experiments were pT<sub>M</sub>RM check failures. A set of four example Arai plots (Nagata et al. 1963) from these experiments that show the range of behaviour observed can be found in the top row of Fig. 1. Approximately half of the specimens that passed our selection criteria had a pT<sub>M</sub>RM failure in the highest (not accepted) power integral ranges. Zigzag was visually observed in 14/41 (34 per cent) specimens (Fig. 1, top row), with the zigzag often increasing after a pT<sub>M</sub>RM failure. In no case was the zigzag alone sufficient for the Arai plot data to have unacceptably high scatter  $(\beta)$ .

We ran 17 specimens from section 1 using MW-Perp with an 88 per cent success rate. The two failures for the MW-Perp experiments were the result of the angle  $(\theta_1 + \theta_2)$  between the total vector and NRM  $(\theta_1)$  and the total vector and  $B_{lab}$   $(\theta_2)$  (Hill & Shaw 2007) exceeding the tolerance allowed. This kind of failure can be attributed to anisotropy, alteration, or imperfect removal of any overprints (which results in a non-perpendicular field direction). We found an average PI of  $31.2 \pm 5.0 \, \mu T$ . The middle row of Fig. 1 demonstrates that although the plots are often very straight, the estimates are still biased to lower values.

As an intermediate between MW-IZZI+ and MW-Perp, we ran 12 specimens using MW-Perp++ , with a below average success rate of 50 per cent. Like the MW-IZZI+ specimens, the most common reason for failure was  $pT_MRM$  check failures. Like this section's MW-IZZI+ specimens, half of the specimens that passed the selection criteria had a  $pT_MRM$  failure in the highest (not accepted) power integrals. These specimens gave an estimate falling between that of the MW-IZZI+ and MW-Perp, at  $33.5\pm1.9~\mu T$ . The bottom row of Fig. 1 demonstrates that the MW-Perp++ also has Arai plots with data characteristics between those of MW-IZZI+ and MW-Perp.

### 3.1.2 Section 2

Section 2 gave higher estimates than section 1 and showed relatively consistent results from all three protocols. 18 specimens received an MW-IZZI+ treatment. 14 specimens (78 per cent) passed the loose selection criteria, 11 specimens (61 per cent) passed the moderately strict selection criteria and 3 specimens (17 per cent) passed the strict selection criteria. These gave the highest average PI estimates at 41.7  $\pm$  6.5, 39.8  $\pm$  4.6 and 43.9  $\pm$  8.9  $\mu$ T, respectively. The estimate givn by the loose selection criteria is statistically distinct from the expected value 36.2  $\mu$ T (p = 0.010), but the moderately strict (p = 0.090) and strict estimates are not (p = 0.29). All the specimens that failed, did so because of pT<sub>M</sub>RM check failures. Half of the specimens that passed had pT<sub>M</sub>RM failures at higher (not-accepted) power integrals. The top row of Fig. 2 contains representative Arai plots from these data. Slight zigzag was observed in 5/18 (36 per cent) Arai plots, with minimal observed change after pT<sub>M</sub>RM failures.

Of the eight specimens that received an MW-Perp treatment, five passed. The three failures were, like for specimens from section 1, the result of the  $\theta_1 + \theta_2$  angle exceeding tolerance. The successful

Table 1. Selection criteria.

						→			$DRAT^b$	
Type	N	FRAC	$R^2$	β	q	K'	$\mathrm{MAD}_{\mathrm{ANC}^{\mathrm{a}}}$	αa	(per cent)	$\Delta  heta^{ extsf{c}}$
Loose <sup>d</sup>	≥4	_	≥0.9	_	_	-	≤10	_	≤10	_
Moderate	≥4	≥0.45	_	<b>≤</b> 0.1	≥4	<b>≤</b> 0.480	<u>≤</u> 10	≤10	≤10	≤0.25°
Strict <sup>d</sup>	≥4	≥0.78	_	≤0.1	≥4	≤0.164	≤5	≤10	≤10	_

<sup>&</sup>lt;sup>a</sup>For technical reasons, only IZZI+ data can use these criteria.

**Table 2.** New palaeointensity estimates.

	Section 1 PI estimate Median		Success rate (per		Section 2 PI estimate	Median	Success rate (per	
Method	$(\mu T \pm 1\sigma)$	$\beta$ (passed $\pm 1\sigma$ )	cent)	N	(μT)	$\beta$ (passed $\pm 1\sigma$ )	cent)	N
MW-Perp	$31.2 \pm 5.0$	$0.0354 \pm 0.015$	88	15	$37.7 \pm 5.4$	$0.0395 \pm 0.028$	63	5
MW-Perp++	$33.5 \pm 1.9$	$0.0394 \pm 0.0068$	50	6	$36.8 \pm 5.7$	$0.0295 \pm 0.016$	89	8
MW-IZZI+ (loose)	$37.3 \pm 3.3$	$0.0615 \pm 0.024$	70	29	$41.7 \pm 6.5$	$0.0628 \pm 0.028$	78	14
MW-IZZI+ (moderate)	$36.8 \pm 3.4$	$0.0571 \pm 0.022$	54	22	$39.1 \pm 4.6$	$0.0692 \pm 0.027$	61	11
MW-IZZI+ (strict)	_	_	_	0	$43.9 \pm 8.9$	$0.0490 \pm 0.036$	17	3

experiments gave an average PI estimate of  $37.7 \pm 5.4~\mu T$ . The bottom row of Fig. 2 shows half of the accepted Arai plots from section 2's MW-Perp data set.

Like with section 1, the MW-Perp++ PI estimates for section 2 falls between that of the MW-IZZI+ and the MW-Perp. Only one specimen out of nine failed, as a result of its pT<sub>M</sub>RM checks failing. Of the specimens that passed, two had pT<sub>M</sub>RM failure at the highest (not accepted) power integrals. The successful specimens gave an average of  $36.8 \pm 5.7~\mu T$ . Representative Arai plots can be found in the middle row of Fig. 2.

### 3.2 Interpreting MW-IZZI+ as MW-Perp and MW-Perp++

The MW-IZZI+ experiments were run perpendicular to each specimen's NRM direction. For the derived MW-Perp++ (MW-derPerp++) test, we removed the first Z step data from each ZI-IZP couplet and treated the rest of the data as normal for MW-Perp++. For the derived MW-Perp (MW-derPerp) test, we removed all the Z and P steps from the raw data file. We then processed these data through the same plotting routine as the MW-Perp and MW-Perp++ data. Many specimens failed due to the angle changing, which was also observed in our real MW-Perp experiments.

From the MW-derPerp++ Arai plots (examples in Fig. 3), we found an average PI estimate of  $33.2 \pm 5.8~\mu T$  (28/41 passed) for section 1 and  $39.9 \pm 8.2~\mu T$  (10/18 passed) for section 2. These estimates are not statistically distinct from the (direct) MW-Perp++ estimates and are on average 10 per cent lower and 2 per cent higher than the respective MW-IZZI+ estimates. The MW-IZZI+ estimate for section 1 is statistically distinct from section 1 MW-derPerp++ estimate; section 2 estimates are not statistically distinct. Fig. 3 compares the specimen-level MW-derPerp++ PI estimates with the MW-IZZI+ data from which the MW-derPerp++ data are derived. Table 3 contains a comparison of the MW-derPerp++ mean with the MW-IZZI+ and MW-Perp++ means.

From the MW-derPerp Arai plots (examples in Fig. 4), we extracted an average PI estimate of  $31.3\pm4.6~\mu T~(32/41~passed)$  for section 1 and  $37.1\pm9.9~\mu T~(13/18~passed)$  for section 2. Using the MW-IZZI+ data without pT\_MRM checks or Z steps gave PI estimates that are not statistically distinct from and are within 4 per cent our MW-Perp estimates of 31.2 and 37.7  $\mu T$ , respectively (but are from each other). The estimates are 15 and 8.7 per cent lower than the respective MW-IZZI+ site-level estimates. Fig. 4 compares the specimen-level MW-derPerp PI estimates with the MW-IZZI+ data from which the MW-derPerp data are derived. Table 3 contains a comparison of the MW-derPerp mean with the MW-IZZI+ and MW-Perp means.

### 3.3 Using the MW-IZZI+ data to interpret the MW-Perp data

To try to remove the effects of alteration on the PI estimates, we repeated the analysis of the MW-Perp with the additional constraint that we only allowed data from power integrals below which  $pT_MRM$  checks in MW-IZZI+ sister specimens did not fail. We extracted PI estimates of 34.6  $\pm$  4.7  $\mu T$  (14/17 passed) for section 1 and 41.0  $\pm$  7.0 (6/8 passed) for section 2. These estimates are not statistically different from their respective MW-IZZI+ , MW-Perp++ , or MW-Perp estimates. Assuming sister specimens had alterations occur at similar power integrals, this observation implies that undetected alterations caused a shallowing of the Arai plot, which caused PI estimates to be lower than expected.

### 3.4 pT<sub>M</sub>RM checks versus hysteresis parameters

This experiment aims to test if changes observing hysteresis parameters are sufficient to identify alterations when pT<sub>M</sub>RM checks are not present (Hill & Shaw 2000). We ran six specimens, three from section 1 and three from section 2 to compare the changes in the hysteresis parameters of the specimens with the results of pT<sub>M</sub>RM checks measured during a series of treatments that mimicked a PI experiment. Fig. 5 contains the results of this experiment (the reader

<sup>&</sup>lt;sup>b</sup>Perpendicular data lack pT<sub>M</sub>RM checks, so DRAT cannot be used for these data.

<sup>&</sup>lt;sup>c</sup>Used only for perpendicular-style experiments.

<sup>&</sup>lt;sup>d</sup>These criteria were only tested on MW-IZZI+ data.

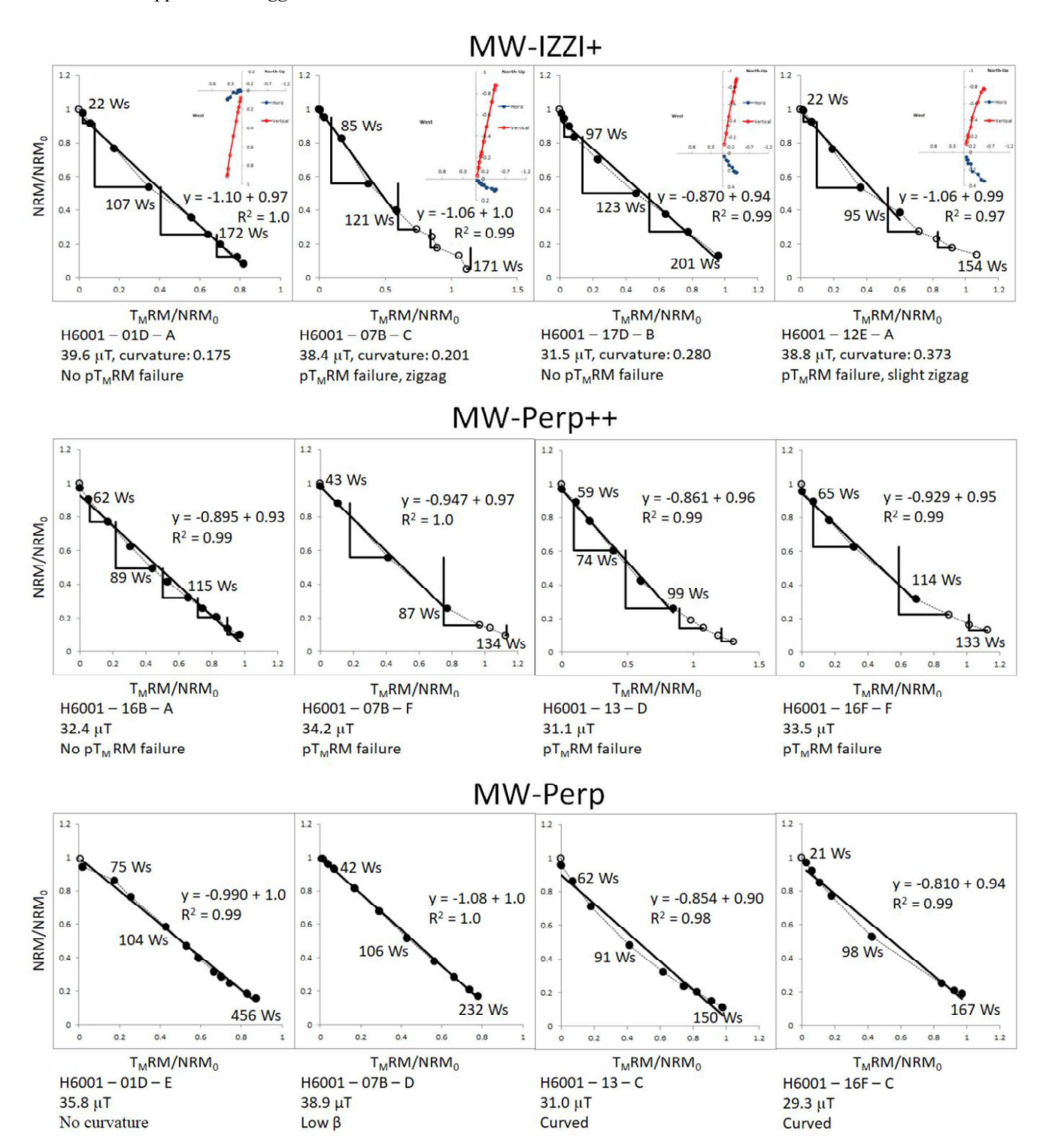


Figure 1. Section 1 Arai plot examples. Orthogonal projections are provided for MW-IZZI+ data. Black circles are accepted data points (with their line of best fit in black), open circles are rejected data points (using the moderately strict selection criteria). The black right-angled lines are  $pT_MRM$  checks, and  $\beta$  is a measure of data scatter around the best fit line. Evidence of alteration was found in approximately half of specimens that had  $pT_MRM$  checks. The MW-Perp specimens have some of the most linear Arai plots but on average also gave the lowest PI estimate.

is referred to Supporting Information Section A.2 for further discussion). All specimens exhibited a trend to move towards the single domain region as the applied power increased. The dotted lines cor-

respond to failed  $pT_MRM$  checks and the solid lines correspond to positive  $pT_MRM$  checks for sister specimens. The largest changes in hysteresis parameters generally corresponded to  $pT_MRM$  check failures. The correlation, however, is insufficiently quantified to be used in place of  $pT_MRM$  checks.

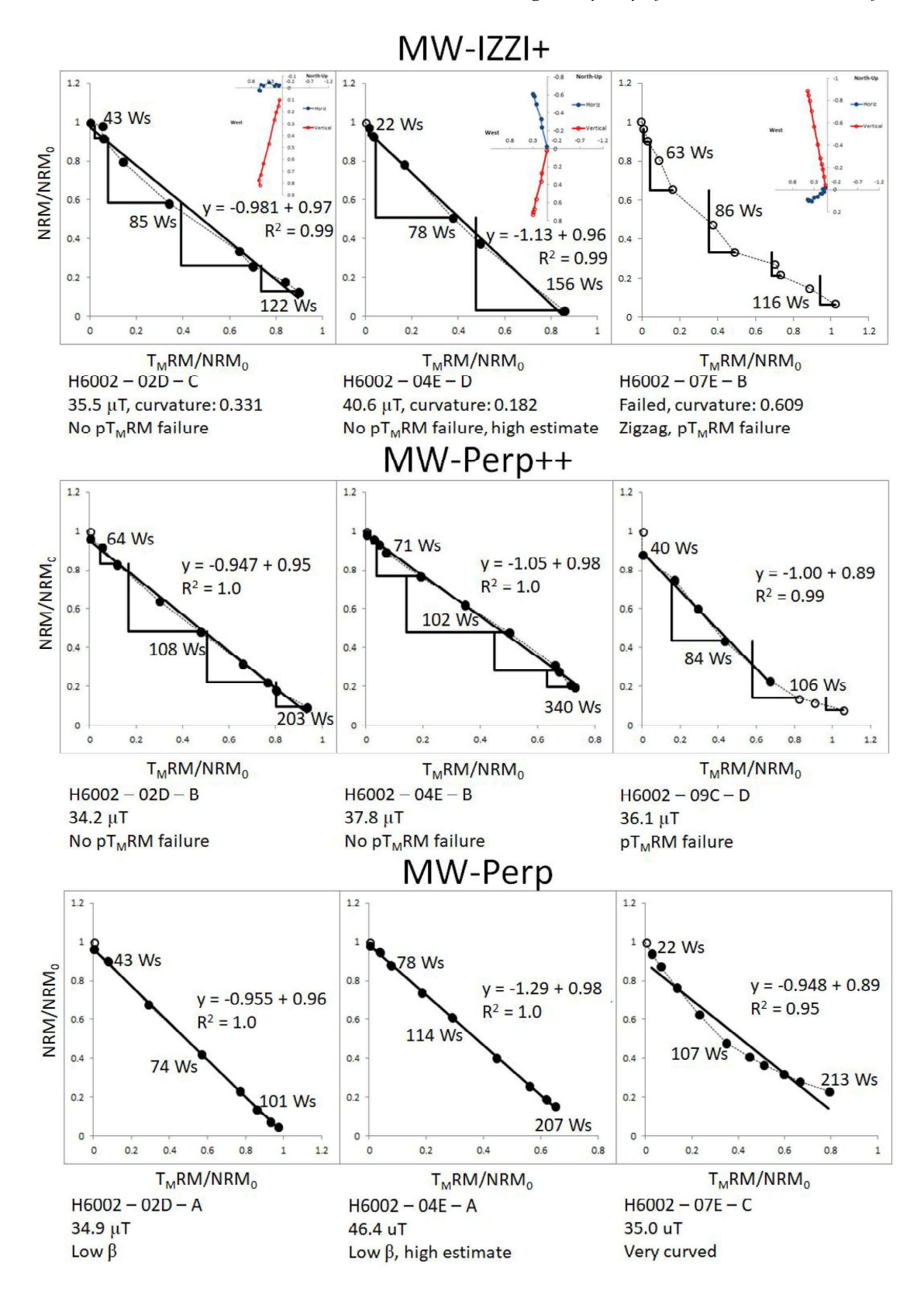


Figure 2. Section 2 Arai plot examples. Orthogonal projections are provided for MW-IZZI+ data. Black circles are accepted data points (with their line of best fit in black), open circles are rejected data points (using the moderately strict selection criteria). The black right-angled lines are  $pT_MRM$  checks, and  $\beta$  is a measure of data scatter around the best fit line. The Arai plots for specimens in section 2 had similar behaviour to those in section 1 in terms of  $pT_MRM$  failures and zigzagging MW-IZZI+ Arai plots.

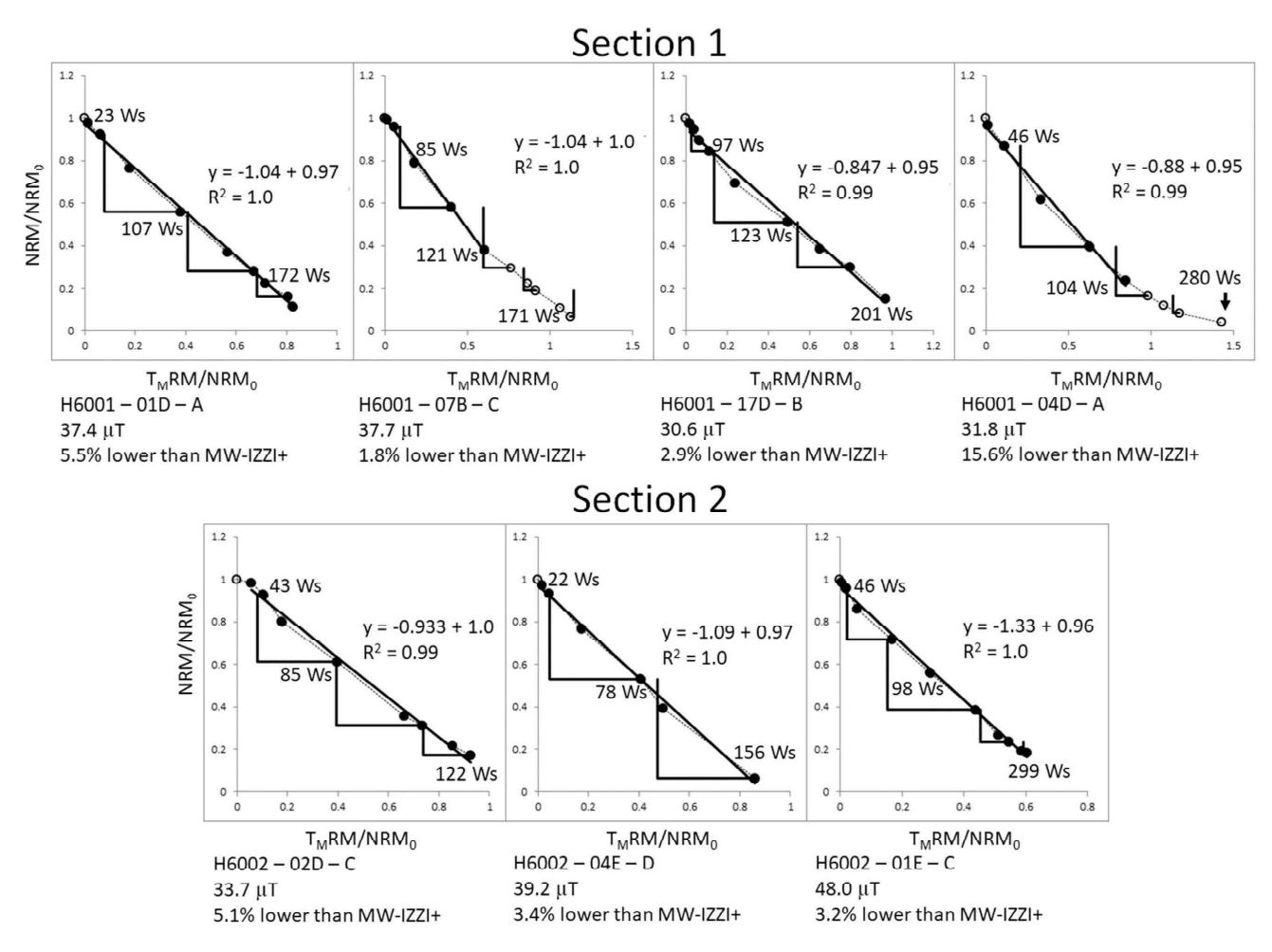


Figure 3. MW-IZZI+ data interpreted as MW-Perp++ (MW-derPerp++) data; appropriate Z steps were removed and then the raw data were replotted. Black circles are accepted data points (with their line of best fit in black), open circles are rejected data points. The black right-angled lines are pT<sub>M</sub>RM checks. Top: section 1 (section average with this treatment:  $33.2 \pm 5.8 \mu$ T). Bottom: section 2 (section average with this treatment:  $39.9 \pm 8.2 \mu$ T).

**Table 3.** Estimates extracted by section and protocol.

Method	Section 1 PI estimate ( $\mu$ T)	IEF	N	Section 2 PI estimate ( $\mu$ T)	IEF	N
MW-Perp (new)	$31.2 \pm 5.0$	0.16	15	$37.7 \pm 5.4$	0.031	5
MW-Perp++ (new)	$33.5 \pm 1.9$	0.081	6	$36.8 \pm 5.7$	0.016	8
MW-IZZI+ (new, loose)	$37.3 \pm 3.3$	0.030	29	$41.7 \pm 6.5$	0.15	14
MW-IZZI+ (new, moderate)	$36.8 \pm 3.4$	0.016	22	$39.1 \pm 4.6$	0.074	11
MW-IZZI+ (new, strict)	_	_	0	$43.9 \pm 8.9$	0.21	3
MW-IZZI+ (treated as MW-Perp in Section 3.2)	$31.3 \pm 4.6$	0.016	32	$37.1 \pm 9.9$	0.024	13
MW-IZZI+ (treated as MW-Perp++ in Section 3.2)	$33.2 \pm 5.8$	0.090	28	$39.9 \pm 8.2$	0.093	10
MW-Perp (treated as in Section 3.3)	$34.6 \pm 4.7$	0.046	14	$41.0 \pm 7.0$	0.12	6
MW-Perp	$31.6 \pm 3.6  (all)$	0.15	40	$37.1 \pm 6.4  (all)$	0.024	30
(Hill & Shaw 2000)	$31.2 \pm 3.4  (sister)$	0.16	22	$35.9 \pm 5.5  (sister)$	0.008	14
MW-Perp (treated as in Section 4.2)	$33.4 \pm 5.8$	0.084	21	$36.3 \pm 6.4$	0.003	14

Note: N is the number of specimens across all samples from the section. IEF is the intensity error fraction (Biggin et al. 2007).

### 4 DISCUSSION

### 4.1 Non-SD behaviour

The overall goal was to find estimates as close to 36.2–36.5  $\mu T$  as possible, while minimizing the unnecessary rejection of measurement-level Arai plot data. Our closest estimate from section 1 was produced by MW-IZZI+ experiments and the closest estimate from section 2 came from its MW-Perp++ experiments

(all estimates can be found in Table 3). Section 2 was previously shown in Hill & Shaw (2000) to exhibit two-slope behaviour in its Arai plots. We have found the inflection point for their two-sloped Arai plots to be correlated with  $pT_MRM$  check failures when present. The mean curvatures,  $|\overrightarrow{K}'|$ , for sections 1 and 2 are 0.283 and 0.261, respectively, which are relatively high. Curved Arai plots are the characteristic of specimens containing non-SD grains (Levi 1977; Shcherbakov & Shcherbakova 2001; Biggin

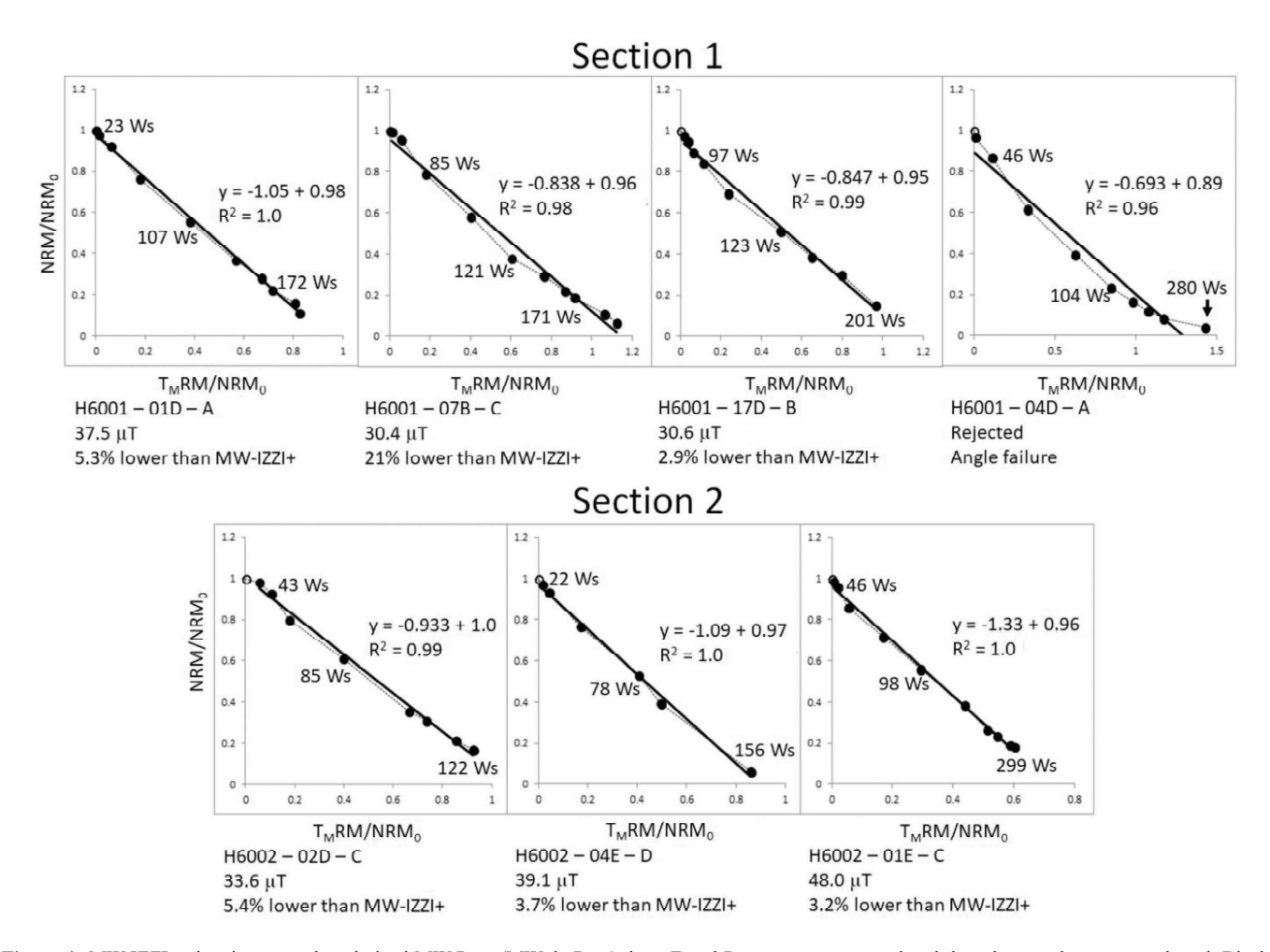


Figure 4. MW-IZZI+ data interpreted as derived MW-Perp (MW-derPerp) data; Z and P steps were removed and then the raw data were replotted. Black circles are accepted data points (with their line of best fit in black), open circles are rejected data points. The black right-angled lines are pT<sub>M</sub>RM checks. Top: section 1 (section average with this treatment:  $31.3 \pm 4.6 \,\mu$ T). Bottom: section 2 (section average with this treatment:  $37.1 \pm 9.9 \,\mu$ T).

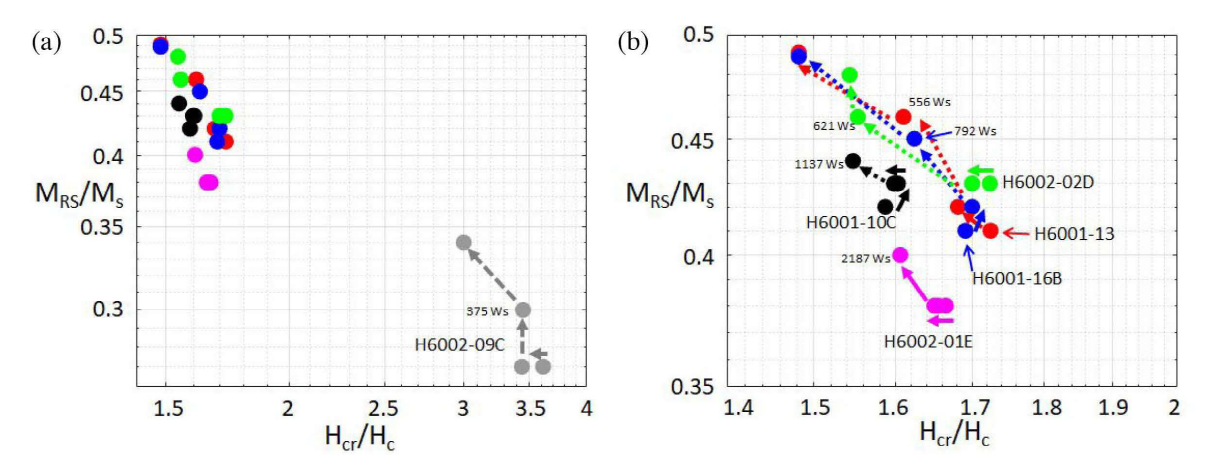


Figure 5. Hysteresis parameter plot showing movement over a simulated MW-IZZI+ experiment. (a) All data taken and (b) zoomed in near the S.D. section. Solid coloured arrows correspond to a passed  $pT_MRM$  check on sister specimens, whereas dotted coloured arrows correspond to a failed  $pT_MRM$  check on sister specimens. Power integrals are noted at the first failed  $pT_MRM$  check or highest power integral step.

2010; Hodgson *et al.* 2018). The  $pT_MRM$  check failures in the MW-Perp++ data are consistent with the findings in Biggin (2010), who found that  $pT_MRM$  checks can exaggerate non-SD behaviour. The MW-derPerp++ data have  $pT_MRM$  check failures at similar power integrals and NRM remaining to the MW-IZZI+ data. We interpret

the  $pT_MRM$  check failures to be the result of irreversible thermochemical alteration, but the data also indicate non-SD behaviour as a potential source of error. The zigzagging Arai plots found in more than 1/3 of all new specimens given an IZZI+ treatment; this is also the characteristic of non-SD grains.

### 4.2 Comparison with previous microwave results

Our new MW-Perp estimates agree very closely with those from Hill & Shaw (2000). For section 1, we extracted an estimate of  $31.2\pm5.0~\mu\text{T}$ , compared to their overall estimate of  $31.6\pm3.6~\mu\text{T}$ . For section 2, we extracted an estimate of  $37.7\pm5.4$ , compared to their overall estimate of  $37.1\pm6.4$ . If we look only at estimates from the exact same core samples, Hill & Shaw (2000) extracted estimates of  $31.2\pm3.4~\mu\text{T}$  and  $36.6\pm7.1~\mu\text{T}$ , differences of <1 and 3 per cent, respectively. Like Hill & Shaw (2000), we found that specimens from section 1, on average, had straighter Arai plots than section 2. Even though we used a different MW system, the 14 GHz Tristan system, instead of the original 8 GHz system Hill & Shaw (2000) used, we still recovered the same MW-Perp estimates, so equipment effects appear to be negligible.

In section 3.3, we used our MW-IZZI+ power integrals and pT<sub>M</sub>RM checks to select MW-Perp Arai plot points. Here we reanalyse the Hill & Shaw (2000) data to independently verify the results. Hill & Shaw (2000) used a different resonant cavity, so we cannot use the power integrals directly like in section 3.3. Instead, we can estimate the power integrals of the pT<sub>M</sub>RM check failures on the Arai plots using the NRM remaining as a rough analogue. For example, if MW-IZZI+ specimen had a failed pT<sub>M</sub>RM check when 40 per cent of the NRM remained, then we only accept MW-Perp data points from Hill & Shaw (2000) that have at least 40 per cent NRM remaining. Following this method, we extracted estimates of  $33.4 \pm 5.8$  and  $36.3 \pm 6.4$   $\mu$ T for sections 1 and 2, respectively, which are < 2 per cent different from our new MW-Perp++ estimates of 33.5  $\pm$  1.9 and 36.8  $\pm$  5.7  $\mu$ T, respectively. The lower estimates observed in MW-Perp compared to MW-Perp++ are, therefore, likely the result of undetected alterations in the MW-Perp data. In the original study of Hill & Shaw (2000), it appears that non-SD and alteration effects were cancelling one another out to a degree such that section 2 fortuitously recovered the PI accurately when the entire (curved) Arai plot was used.

MW-IZZI+ data, with moderately strict selection criteria, for both sections 1 and 2 produce PI estimates that are not statistically distinct ( $p_1 = 0.417$ ;  $p_2 = 0.063$ ) from the 36.2  $\mu$ T value given by the IGRF (Thebault *et al.* 2015). The data with loose selection criteria give overestimates, which is broadly consistent with the findings of Herrero-Bervera & Valet (2009). The data with strict selection criteria give the smallest data set, which means the data likely do not sample the flow sufficiently (Biggin *et al.* 2003). The high scatter, with inaccurate values both above and below the expected value, is consistent with the findings of Paterson *et al.* (2012) that overly strict selection criteria can, in some cases, overly reject accurate data.

Both the new MW-Perp and MW-Perp++ data also give PI estimates that are not statistically different from 36.2  $\mu$ T ( $p_{perp} = 0.85$ ;  $p_{perp++} = 0.77$ ). All new data have intensity error fractions (IEFs) of less than 0.1, except for the new MW-Perp data from section 1, which was expected to have the highest IEF. The new MW-Perp data have IEFs within 0.01 of the data from Hill & Shaw (2000).

The addition of alteration checks in the MW-Perp++ and the data treatment in section 3.3 decrease the IEF of the MW-Perp data in section 1 by 0.08 and 0.11, respectively. These same techniques increase the IEF of the MW-Perp data in section 2 by 0.01 and 0.08, respectively but the new estimates are within uncertainties of the former ones. The low estimates produced by the MW-Perp experiments appears, therefore, to be the result of undetected alterations in the MW-Perp data, rather than a systematic error caused by the MW radiation.

The MW-Perp++ data lack the zigzagging (Yu & Tauxe 2005) of the MW-IZZI+ data, which sometimes allowed more Arai plot data points to be selected. In the case of section 1, selecting additional Arai plot data produced a lower average PI estimate, which mirrors the behaviour seen in the MW-Perp data. For the generally less linear Arai plots in section 2, the different data caused a large increase of dispersion in the PI estimates because different specimens passed the selection criteria.

### 4.3 Implications for similar experiments

When compared to other, thermal studies on this lava flow (e.g. Böhnel  $\it et al. 2011$ ), some of the MW data in Hill & Shaw (2000) appeared to be biased low. The large differences in properties between sections 1 and 2 further obfuscated their results. Cromwell  $\it et al. (2018)$  note this pattern to hold true for all non-thermal Thellier PI experiments for the 0–2 ka age range. We also note, however, that thermal studies from different, often sparsely sampled, sections of the 1960 Kilauea lava flow generally gave PI estimates higher than the 36.5  $\mu T$  field strength observed at the Honolulu Observatory, which probably indicates that the data were affected by exaggerated non-single domain behaviour.

We have demonstrated that MW-IZZI+ experiments can produce results that are highly distinctive from those produced by MW-Perp experiments. With the newest MW system's ability to run any Thellier-style experiment, and the protocol-dependent PI estimates extracted in this paper, MW data should not be combined into a single 'MW method' data set. The new MW Thellier-style results are still lower than those reported in Böhnel *et al.* (2011) and Cromwell *et al.* (2018), but they are not statistically different from the expected values for this lava flow. A direct thermal—microwave comparison is therefore needed in the future on sister specimens.

The lower estimates observed herein for specimens receiving an MW-Perp treatment, compared to MW Thellier-style experiments, are broadly in agreement with Biggin (2010). Biggin (2010), found the largest discrepancies between MW and thermal studies where the MW demagnetization mechanism was coupled with the perpendicular protocol, but the thermal demagnetization mechanism was coupled with a double-heating Thellier-style protocol (see table 2 in Biggin 2010). We have expanded on these results and shown here that low MW-Perp estimates can potentially be the result of both undetected alterations because the Perp protocol lacks pT<sub>M</sub>RM checks as well as the enhanced non-SD behaviour that can be observed in double-heating protocols (Biggin 2010; Hodgson *et al.* 2018).

Whenever relevant rock magnetic data are sparse, our data suggest that the IZZI+ protocol is preferred, as it contains a built-in check for non-SD behaviour and uses  $pT_MRM$  checks. However, as demonstrated in section 2, IZZI+ data can be prone to slight overestimations, so IZZI+, by itself (without any rock magnetism or other independent data), may not always be sufficient for high accuracy PI surveys on older, less well-behaved specimens. Using the MW-IZZI+ data to reinterpret the MW-Perp data gave a PI estimate that was not statistically different from the expected value. The Perp protocol only requires a single treatment at each step, which increases experimental speed and reduces chances for alteration. If the Perpendicular protocol is used, the data set can then be corrected using sister IZZI+ experiments.

A multitechnique approach is favoured when selection criteria have to be more relaxed, due to, for example, the age of the specimens and resulting poorer quality of the Arai plot data. The data herein have showed that running IZZI+ with a perpendicular applied magnetic field allows the data to be interpreted as Perp or Perp++ to have an implicit second protocol to check robustness.

If a multitechnique approach is not possible for technical reasons, then maximizing the number of PI estimates another way is paramount. Multiple sampling sites—to maximize flow coverage, as suggested by Biggin  $et\,al.\,(2007)$ —and reduced-size cores (5 mm diameter  $\times$  1–2 mm height, in our case for microwave specimens), if possible, increase the amount of heterogeneity between specimens. We have seen with these specimens that averaging all these helps approach the correct mean strength of the Earth's magnetic field if previously unrecognized heterogeneities exist.

#### 5 CONCLUSIONS

The modern, 14 GHz Tristan MW system, using the IZZI+ protocol, has yielded PI estimates that are not statistically distinct from the expected values. With the addition of pT<sub>M</sub>RM checks, we have shown that undetected alterations are a primary cause of the lower estimates observed in the MW-Perp data, not a bias resulting from MW radiation or the older system. The MW-IZZI+ protocol has also showed that there is some non-single domain behaviour present in the data. Since the observed alteration mandates using lower 'temperature' (power integral) portions of (subtly) concave Arai plots, some of the PI data appear to be overestimated and often created large Arai plot data point scatter in the MW-Perp and MW-IZZI+ estimates. In addition, we have found that MW-IZZI+ and MW-Perp (with pT<sub>M</sub>RM checks) are reliable protocols in samples with thermochemical alterations because their pT<sub>M</sub>RM checks detect and therefore help mitigate the resulting effect on PI estimates. This non-ideal behaviour appears to be the primary cause of the high estimates and alterations appear to be the primary cause of the lower estimates. Our data herein, therefore, confirm the ability of the MW system to extract accurate PI estimates from samplings that exhibit thermochemical alterations and non-ideal behaviour. The data further demonstrate the utility of both a flexible IZZI protocol and a multiprotocol approach that can be applied to gather large and accurate data sets quickly from basalts that yield fewer ideal data.

### ACKNOWLEDGEMENTS

This study was led by JMG as a portion of a University of Liverpool match-funded studentship, supported by the Duncan Norman Research Scholarship. JMG further acknowledges support from the NERC EAO Doctoral Training Partnership, grant NE/L002469/1 and NERC studentship 1793213. AJB acknowledges support from NERC standard grant NE/P00170X/1 and Leverhulme Research Leadership Award RL-2016-080. JMG thanks Louise Hawkins and the Institute for Rock Magnetism at the University of Minnesota for the use of their facilities to gather FORC data. MJH acknowledges the assistance of John Shaw, Emilio Herrero-Bevera and Don Tarling with the original collection of the examined lava samples. New raw data collected as part of this study will be available on MagIC at earthref.org/MagIC/16586.

### REFERENCES

Biggin, A.J., 2010. Are systematic differences between thermal and microwave Thellier-type palaeointensity estimates a consequence of multidomain bias in the thermal results? *Phys. Earth planet. Inter.*, **180**(1–2), 16.40

- Biggin, A.J., Bohnel, H.N. & Zuniga, F.R., 2003. How many paleointensity determinations are required from a single lava flow to constitute a reliable average? *Geophys. Res. Lett.*, **30**(11).
- Biggin, A.J., Perrin, M. & Dekkers, M.J., 2007. A reliable absolute palaeointensity determination obtained from a non-ideal recorder, *Earth planet*. *Sci. Lett.*, 257(3–4), 545–563.
- Biggin, A.J., Badejo, S., Hodgson, E., Muxworthy, A.R., Shaw, J. & Dekkers, M.J., 2013. The effect of cooling rate on the intensity of thermoremanent magnetization (TRM) acquired by assemblages of pseudo-single domain, multidomain and interacting single-domain grains, *Geophys. J. Int.*, 193(3), 1239–1249.
- Böhnel, H., Herrero-Bervera, E. & Dekkers, M.J., 2011, Paleointensities of the Hawaii 1955 and 1960 lava flows: further validation of the multispecimen method, in *The Earth's Magnetic Interior*, pp. 195–211, eds Petrovský, E., Ivers, D., Harinarayana, T. & Herrero-Bervera, E., Springer.
- Bono, R.K., Tarduno, J.A., Nimmo, F. & Cottrell, R.D., 2019. Young inner core inferred from Ediacaran ultra-low geomagnetic field intensity, *Nat. Geosci.*, 12(2), 143–147.
- Coe, R.S. & Gromme, C.S., 1973. Comparison of 3 methods of determining geomagnetic paleointensities, *J. Geomagn. Geoelectr.*, **25**(4), 415–435.
- Cromwell, G., Tauxe, L., Staudigel, H. & Ron, H., 2015. Paleointensity estimates from historic and modern Hawaiian lava flows using glassy basalt as a primary source material, *Phys. Earth planet. Inter.*, **241**, 44–56.
- Cromwell, G., Trusdell, F., Tauxe, L., Staudigel, H. & Ron, H., 2018. Holocene paleointensity of the island of Hawai'i from glassy volcanics, Geochem. Geophys. Geosyst., 19, 3224–3245.
- Donadini, F., Riisager, P., Korhonen, K., Kahma, K., Pesonen, L. & Snowball, I., 2007. Holocene geomagnetic paleointensities: a blind test of absolute paleointensity techniques and materials, *Phys. Earth planet. Inter.*, **161**(1–2), 19–35.
- Dunlop, D.J. & Ozdemir, O., 2001. Beyond Neel's theories: thermal demagnetization of narrow-band partial thermoremanent magnetizations, *Phys. Earth planet. Inter.*, **126**(1–2), 43–57.
- Ferk, A., Leonhardt, R., Hess, K.U., Koch, S., Egli, R., Krasa, D. & Dingwell, D.B., 2014. Influence of cooling rate on thermoremanence of magnetite grains: identifying the role of different magnetic domain states, *J. geophys. Res.*, **119**(3), 1599–1606.
- Herrero-Bervera, E. & Valet, J.P., 2009. Testing determinations of absolute paleointensity from the 1955 and 1960 Hawaiian flows, *Earth planet. Sci. Lett.*, **287**(3–4), 420–433.
- Hill, M.J. & Shaw, J., 2000. Magnetic field intensity study of the 1960 Kilauea lava flow, Hawaii, using the microwave palaeointensity technique, Geophys. J. Int., 142(2), 487–504.
- Hill, M.J. & Shaw, J., 2007. The use of the 'Kono perpendicular applied field method' in microwave palaeointensity experiments, *Earth Planets Space*, **59**(7), 711–716.
- Hill, M.J., Pan, Y.X. & Davies, C.J., 2008. An assessment of the reliability of palaeointensity results obtained from the Cretaceous aged Suhongtu section, Inner Mongolia, China, *Phys. Earth planet. Inter.*, 169(1–4), 76– 88.
- Hodgson, E., Grappone, J.M., Biggin, A.J., Hill, M.J. & Dekkers, M.J., 2018. Thermoremanent behavior in synthetic samples containing natural oxyexsolved titanomagnetite, *Geochem. Geophys. Geosyst.*, 19(6), 1751– 1766.
- Jackson, A., Jonkers, A.R.T. & Walker, M.R., 2000. Four centuries of geomagnetic secular variation from historical records, *Phil. Trans. R. Soc. Lond.*, A, 358(1768), 957–990.
- Kono, M. & Ueno, N., 1977. Paleointensity determination by a modified Thellier method, *Phys. Earth planet. Inter.*, **13**(4), 305–314.
- Levi, S., 1977. Effect of magnetite particle-size on paleointensity determinations of geomagnetic-field, *Phys. Earth planet. Inter.*, **13**(4), 245–259.
- Nagata, T., Momose, K. & Arai, Y., 1963. Secular variation of geomagnetic total force during last 5000 years, *J. geophys. Res.*, **68**(18), 5277–5281.
- Paterson, G.A., Biggin, A.J., Yamamoto, Y. & Pan, Y., 2012. Towards the robust selection of Thellier-type paleointensity data: the influence of experimental noise, *Geochem. Geophys. Geosyst.*, 13(5), doi:10.1029/2012GC004046.

- Paterson, G.A., Biggin, A.J., Hodgson, E. & Hill, M.J., 2015. Thellier-type paleointensity data from multidomain specimens, *Phys. Earth planet. Inter.*, 245, 117–133.
- Santos, C.N. & Tauxe, L., 2019. Investigating the accuracy, precision, and cooling rate dependence of laboratory-acquired thermal remanences during paleointensity experiments, *Geochem. Geophys. Geosyst.*, 20(1), 383– 397.
- Shaar, R., Ron, N., Tauxe, L., Kessel, R. & Agnon, A., 2011. Paleomagnetic field intensity derived from non-SD: testing the Thellier IZZI technique on MD slag and a new bootstrap procedure, *Earth planet. Sci. Lett.*, **310**(3–4), 213–224.
- Shcherbakov, V.P. & Shcherbakova, V.V., 2001. On the suitability of the Thellier method of palaeointensity determinations on pseudosingle-domain and multidomain grains, *Geophys. J. Int.*, **146**(1), 20–30
- Tanaka, H. & Kono, M., 1991. Preliminary-results and reliability of paleointensity studies on historical and C-14 dated Hawaiian lavas, *J. Geomagn. Geoelectr.*, 43(5), 375–388.
- Thebault, E. *et al.*, 2015. International geomagnetic reference field: the 12th generation, *Earth Planets Space*, **67**, 19, doi:10.1186/s40623-015-0228-9.
- Yamamoto, Y., Tsunakawa, H. & Shibuya, H., 2003. Palaeointensity study of the Hawaiian 1960 lava: implications for possible causes of erroneously high intensities, *Geophys. J. Int.*, 153(1), 263–276.
- Yu, Y., 2011. Importance of cooling rate dependence of thermoremanence in paleointensity determination, *J. geophys. Res.*, 116, doi:10.1029/2011JB008388.

- Yu, Y.J. & Tauxe, L., 2005. Testing the IZZI protocol of geomagnetic field intensity determination, Geochem. Geophys. Geosyst., 6, doi:10.1029/2004GC000840.
- Yu, Y.J., Tauxe, L. & Genevey, A., 2004. Toward an optimal geomagnetic field intensity determination technique, *Geochem. Geophys. Geosyst.*, 5, 18.

### SUPPORTING INFORMATION

Supplementary data are available at GJI online.

**Figure A1.** FORC diagrams for two specimens from section 1: (a) H6001–04A and (b) H6001–09D. Sister specimens of these gave lower than expected PI estimates from Arai plots with some pT<sub>M</sub>RM check failures, so they appear to be characteristic of the specimens tested.

**Table B1.** MW-IZZI+

**Table B2.** MW-Perp++

Table B3. MW-Perp

**Table B4.** MW-Perp(using MW-IZZI+ pTmRM)

Table B5. MW-derPerp

**Table B6.** MW-derPerp++

Please note: Oxford University Press is not responsible for the content or functionality of any supporting materials supplied by the authors. Any queries (other than missing material) should be directed to the corresponding author for the paper.